Plasma Power Source Based on a Catalytic Reaction of Atomic Hydrogen Measured by Water Bath Calorimetry

R. L. Mills, X. Chen, P. Ray, J. He, B. Dhandapani
BlackLight Power, Inc.
493 Old Trenton Road
Cranbury, NJ 08512

ABSTRACT

Extreme ultraviolet (EUV) spectroscopy was recorded on microwave discharges of helium with 2% hydrogen. Novel emission lines were observed with energies of $q \cdot 13.6\ eV$ where $q = 1,2,3,4,6,7,8,9,11$ or these lines inelastically scattered by helium wherein $21.2\ eV$ was absorbed in the excitation of $He\ (1s^2)$ to $He\ (1s^1 2p^1)$. The average hydrogen atom temperature was measured to be $180 - 210\ eV$ versus $\approx 3\ eV$ for pure hydrogen. The electron temperature T_e for helium-hydrogen was 28,000 K compared to 6800 K for pure helium. Dominant He^+ emission and an intensification of the plasma emission observed when He^+ was present with atomic hydrogen demonstrated the role of He^+ as a catalyst. Using water bath calorimetry, excess power was observed from the helium-hydrogen plasma compared to control krypton plasma. For example, for an input of 8.1 W, the total plasma power of the helium-hydrogen plasma measured by water bath calorimetry was 30.0 W corresponding to 21.9 W of excess power in 3 cm^3. The excess power density and energy balance were high, $7.3\ W/cm^3$ and $-2.9\ X\ 10^4\ kJ/mole\ H_2$, respectively.

1. Introduction

A new chemically generated or assisted plasma source has been developed that is based on a resonant energy transfer mechanism (rt-plasma). One such source operates by incandescently heating a hydrogen dissociator and a catalyst to provide atomic hydrogen and gaseous catalyst, respectively, such that the catalyst reacts with the atomic hydrogen to produce a plasma. It was extraordinary that intense EUV emission was observed by Mills et al. [1-2] at low temperatures (e.g. $\approx 10^3\ K$) and an extraordinary low field strength of about 1-2 V/cm from atomic hydrogen and certain atomized elements or certain gaseous ions which singly or multiply ionize at integer multiples of the potential energy of atomic hydrogen, $27.2\ eV$. A number of independent experimental observations confirm that the rt-plasma is due to a novel reaction of atomic hydrogen which produces as chemical intermediates, hydrogen in fractional quantum states that are at lower energies than the traditional "ground" ($n=1$) state. Power is released, and the final reaction products are novel hydride compounds. The supporting data include EUV spectroscopy [1-12], characteristic emission from catalysts and the hydride ion products [3-5], lower-energy hydrogen emission [6-9], chemically formed plasmas [1-5, 10], Balmer α line broadening [2, 5-6, 8, 11-12], anomalous plasma afterglow duration [10], power generation [6, 11], and analysis of novel chemical compounds [13-16].

The reaction has applications as a new light source, a new field of hydrogen chemistry, and a new source of energy. Since the power is in the form of a plasma, direct plasma to electric power conversion is possible. Plasmadynamic conversion of microwave plasma power to electricity has been achieved at about 3.6W/ cm^3 with about 42% efficiency [17].

The theory given previously [18-20] is based on applying Maxwell's equations to the Schrödinger equation. The familiar Rydberg equation (Eq. (1)) arises for the hydrogen excited states for $n>1$ of Eq. (2).

$$E_n = -\frac{e^2}{n^2 8\pi\varepsilon_o a_H} = -\frac{13.598\ eV}{n^2} \tag{1}$$

$$n = 1,2,3,... \tag{2}$$

An additional result is that atomic hydrogen may undergo a catalytic

reaction with certain atoms and ions which singly or multiply ionize at integer multiples of the potential energy of atomic hydrogen, $m \cdot 27.2\,eV$ wherein m is an integer. The reaction involves a nonradiative energy transfer to form a hydrogen atom that is lower in energy than unreacted atomic hydrogen that corresponds to a fractional principal quantum number. That is

$$n = \frac{1}{2}, \frac{1}{3}, \frac{1}{4}, ..., \frac{1}{p}; \quad p \text{ is an integer} \tag{3}$$

replaces the well known parameter $n = \text{integer}$ in the Rydberg equation for hydrogen excited states. The $n = 1$ state of hydrogen and the $n = \frac{1}{\text{integer}}$ states of hydrogen are nonradiative, but a transition between two nonradiative states, say $n = 1$ to $n = 1/2$, is possible via a nonradiative energy transfer. Thus, a catalyst provides a net positive enthalpy of reaction of $m \cdot 27.2\,eV$ (i.e. it resonantly accepts the nonradiative energy transfer from hydrogen atoms and releases the energy to the surroundings to affect electronic transitions to fractional quantum energy levels). As a consequence of the nonradiative energy transfer, the hydrogen atom becomes unstable and emits further energy until it achieves a lower-energy nonradiative state having a principal energy level given by Eqs. (1) and (3). Processes such as hydrogen molecular bond formation that occur without photons and that require collisions are common [21]. Also, some commercial phosphors are based on resonant nonradiative energy transfer involving multipole coupling [22].

We propose that atomic hydrogen may undergo a catalytic reaction with He^+ which ionizes at two times the potential energy of atomic hydrogen, $2 \cdot 27.2\,eV$. Thus, microwave discharges of helium-hydrogen mixtures were studied by EUV spectroscopy to search for line emission from transitions to fractional Rydberg states of atomic hydrogen. Since the electronic transitions are very energetic, Balmer α line broadening, electron temperature, and power balances were measured to determine whether this reaction has sufficient kinetics to merit its consideration as a practical power source.

2. Experimental

EUV spectroscopy was recorded on hydrogen, xenon, helium, xenon-hydrogen (98/2%), and helium-hydrogen (98/2%) microwave discharge plasmas (Opthos, Model MPG-4M, Frequency: 2450 MHz) according to the methods given previously [7]. The experimental set up comprising a microwave discharge gas cell light source and an EUV spectrometer which was differentially pumped is shown in Figure 1. A xenon-hydrogen (98/2%) or helium-hydrogen (98/2%) gas mixture was flowed at 1 Torr or 20 Torr through a half inch diameter quartz tube fitted with an Evenson cavity, and each plasma of hydrogen, xenon, and helium alone was run at 20 Torr. The input power to the plasma was set at 85 W with forced air cooling of the cell. The spectrometer was a normal incidence 0.2 m monochromator equipped with a 1200 lines/mm holographic grating with a platinum coating that covered the region $2-560\,nm$. The EUV spectrum was recorded with a CEM. The wavelength resolution was about $0.02\,nm$ (FWHM) with slit widths of $50\,\mu m$. The increment was $0.2\,nm$ and the dwell time was $500\,ms$. Peak assignments were based on a calibration against the known He I and He II lines.

To achieve higher sensitivity at the shorter EUV wavelengths, the light emission from microwave plasmas of helium alone was recorded with a 4° grazing incidence EUV spectrometer equipped with a grating having 600 G/mm with a radius of curvature of $\approx 1\,m$ that covered the region $5-65\,nm$. The monochromator angle of incidence was 87°. The resolution was about $0.04\,nm$ (FWHM) with slit widths of $300\,\mu m$. A CEM was used to detect the EUV light. The increment was $0.1\,nm$ and the dwell time was $1\,s$. In addition, the intensity of the emission of the He II peak at $30.4\,nm$ was compared to that of the He I peak at $58.4\,nm$ with the addition of 5% hydrogen to a helium microwave plasma at 1 Torr. The emission was recorded with the 4° grazing incidence EUV spectrometer.

The width of the 656.3 nm Balmer α line emitted from hydrogen alone, xenon-hydrogen mixture (90/10)%, and helium-hydrogen mixture (90/10)% microwave discharge plasmas was measured with a high resolution visible spectrometer capable of a resolution of $\pm 0.006\,nm$ over the spectral range 190-860 nm [11-12]. The plasma emission was fiber-optically coupled through a 220F matching fiber adapter positioned 2 cm

from the cell wall to a Jobin Yvon Horiba 1250 M spectrometer with 2400 groves/mm ion-etched holographic diffraction grating. The entrance and exit slits were set to $20\,\mu m$. The spectrometer was scanned between 655.5-657.0 nm using a 0.005 nm step size. The signal was recorded by a PMT with a stand alone high voltage power supply (950 V) and an acquisition controller. The data was obtained in a single accumulation with a 1 second integration time. The total pressure was 1 Torr, and the input power to the plasma was set at 40 W.

T_e was measured on 0.1 Torr microwave plasmas of helium alone and helium-hydrogen mixtures (90/10%) from the ratio of the intensity of the *He* 501.6 nm (upper quantum level n=3) line to that of the *He* 492.2 nm (n=4) line as described by Griem [23]. T_e was measured on hydrogen alone plasmas from their Balmer line intensities. The visible spectrum $400-560\,nm$ was recorded with the normal incidence EUV spectrometer using a PMT and a sodium salicylate scintillator.

The intensity of the hydrogen Lyman and Balmer emission was measured with the addition of 5% helium to a hydrogen glow discharge plasma. A diagram of a discharge cell light source and the experimental setup for discharge measurements is illustrated in Figure 2. A hollow cathode and EUV spectrograph were aligned on a common optical axis using a laser. The vacuum ultraviolet emission spectrum was obtained for hydrogen and helium-hydrogen (5/95%) plasma with a gas discharge cell that comprised a five-way stainless steel cross that served as the anode with a hollow stainless steel cathode. The plasma was generated at the hollow cathode (0.5 cm ID) inside the discharge cell. The hollow cathode was constructed of a stainless steel rod inserted into a steel tube, and this assembly was inserted into an Alumina tube. A flange opposite the end of the hollow cathode connected the spectrometer to the cell. It had a small hole that permitted radiation to pass to the spectrometer. An AC power supply (0 - 1 kV, 0 - 100 mA) was connected to the hollow cathode to generate a discharge. The AC voltage and current at the time the EUV spectrum was recorded were 200 V and 40 mA, respectively. A Swagelok adapter at the very end of the steel cross provided a gas inlet and a connection with the pumping system, and the cell was pumped with a mechanical pump. Valves were located between the cell and the mechanical pump, the cell and the monochromator, and the

monochromator and its turbo pump. The five-way cross was pressurized with 400 mtorr of gas which was maintained by flowing hydrogen or helium-hydrogen (5/95%) while monitoring the pressure with a 1 torr absolute pressure gauge. The Lyman and Balmer emission was recorded with the normal incidence EUV spectrometer and the high resolution visible spectrometer, respectively.

The excess power was measured by water bath calorimetry on helium-hydrogen (90/10%) plasmas compared to krypton plasma with the same input power. The plasmas were maintained in a microwave discharge cell shown in Figure 3. Each gas was ultrahigh pure. Each pure test gas was flowed through a half inch diameter quartz tube at 500 mTorr maintained with a noble gas or hydrogen flow rate of 10 sccm. After the calorimeter had reached a steady state, the pressure of the helium-hydrogen mixture was changed to 0.29 torr. Each gas flow was controlled by a 0-20 sccm range mass flow controller (MKS 1179A21CS1BB) with a readout (MKS type 246). The cell pressure was monitored by a 0-10 Torr MKS Baratron absolute pressure gauge. The tube was fitted with an Evenson coaxial microwave cavity (Opthos) having an E-mode [24-25]. The microwave generator shown in Figure 3 was an Opthos model MPG-4M generator (Frequency: 2450 MHz).

The Evenson cavity and a plasma-containing section of the quartz tube were fitted with a water-tight stainless steel housing shown in Figure 3. The housing comprised a 4X4X2 cm rectangular enclosure welded to a set of high vacuum 15.24 cm diameter conflat flanges. A silver plated copper gasket was placed between a mating flange and the cell flange. The two flanges were clamped together with 10 circumferential bolts. The top mating flange contained two penetrations comprising 1.) a stainless steel thermocouple well (1 cm OD) housing a thermocouple probe in the cell interior that was in contact with the quartz tube wall adjacent to the Evenson cavity and 2.) a centered 2.54 cm OD coaxial cable housing. The 1.27 cm OD quartz tube was sealed at its penetrations with the rectangular housing by Ultratorr fittings. The housing and cell assembly was suspended by 4 support rods from an 5.1 cm thick acrylic plate which held the cell vertically from the top of a water bath calorimeter shown in Figure 3. The plate contained four sealed penetrations comprising 1.) the stainless steel thermocouple well

2.) a 1 cm OD noble or hydrogen gas line, 3.) a 1 cm OD vacuum line, and 4.) the 2.54 cm OD coaxial cable housing. The gas inlet connected to a 0.64 cm OD flexible stainless steel tube that was connected by an Ultratorr seal to a welded-in 0.63 cm OD penetration of the rectangular enclosure. Inside of the enclosure, the penetration connected to the quartz tube by a 0.63-to-1.27 cm OD mating Ultratorr seal. The quartz tube had an elbow at the end opposite to the gas inlet penetration which attached to a 1 cm OD flexible stainless steel tube section of the vacuum line. The microwave cavity contained in the rectangular enclosure was tuned by a threaded tuning stub sealed in an end wall of the enclosure and a sliding tuning stub sealed with an Ultratorr fitting in the bottom wall. The sliding stub was tightened after the cell was tuned outside of the water bath, and the cell was immersed.

The water bath comprised an insulated reservoir filled with 45 liters of distilled water. The water was agitated with a paddle driven by a stirring motor. A high precision linear response thermistor probe (Omega OL-703) recorded the temperature of the water bath as a function of time for the stirrer alone to establish the baseline. The water bath was calibrated by a high precision heater (Watlow 125CA65A2X, with a Xantrex DC power supply 0-1200 ± 0.01 W). The heat capacity was determined for several input powers, 30, 40, and 50 W ± 0.01 W, and was found to be independent of input power over this power range within ± 0.05%. The temperature rise of the reservoir as a function of time gave a slope in °C/s. This slope was baseline corrected for the negligible stirrer power and loss to ambient. The constant known input power (J/s), was divided by this slope to give the heat capacity in J/°C. Then, in general, the total power output from the cell to the reservoir was determined by multiplying the heat capacity by the rate of temperature rise (°C/s) to give J/s.

Since the cell and water bath system were adiabatic, the general form of the power balance equation is:

$$P_{in} + P_{ex} - P_{out} = 0 \qquad (4)$$

where P_{in} is the microwave input power, P_{ex} is the excess power generated from the hydrogen catalysis reaction, and P_{out} is the thermal power loss from the cell to the water bath. The cell typically reached steady state in about 10 minutes after each experiment was started. At

this point, the power lost from the cell P_{out} was equal to the power supplied to the cell, P_{in}, plus any excess power P_{ex}.

$$P_{in} + P_{ex} = P_{out} \tag{5}$$

Since the cell was surrounded by water that was contained in an insulated reservoir with negligible thermal losses, the temperature response of the thermistor T as a function of time t was modeled by a linear curve

$$\dot{T}(t) = a^{-1} P_{out} \tag{6}$$

where a is the heat capacity (J/°C) for the least square curve fit of the response to power input for the control experiments ($P_{ex} = 0$). The slope was recorded for about 2 hours after the cell had reached a thermal steady state, to achieve an accuracy of ± 1%.

The slope of the temperature rise as a function of time was recorded for each run and baseline corrected for the negligible stirrer power and loss to ambient, then the output power was calculated from the corrected slope. After the calorimeter was calibrated, $T(t)$ was recorded with a selected setting of the forward and reflected power to the krypton plasma. The slope was determined with this constant forward and reflected microwave power, and the microwave input power was absolutely determined for these panel meter readings using Eq. (6) with the $\dot{T}(t)$ response and the heat capacity a. Then, identical forward and reflected microwave power settings were replicated for the helium-hydrogen mixture and $T(t)$ was again recorded. The higher slope produced with helium-hydrogen mixture, having He^+ as a catalyst and atomic hydrogen as a reactant, compared with controls with no hydrogen and no catalyst present was representative of the excess power. In the case of the catalysis run, the total output power P_{out} was determined by solving Eq. (6) using the measured $\dot{T}(t)$ and the heat capacity a. The excess power P_{ex} was determined from Eq. (5). The integral of the excess power P_{ex} over time gave the excess energy E_{ex}.

3. Results and discussion

A. EUV Spectroscopy

In the case of the EUV spectrum of hydrogen, xenon, or xenon-

hydrogen (98/2%), no peaks were observed below 78 *nm*, and no spurious peaks or artifacts due to the grating or the spectrometer were observed. Only known He I and He II peaks were observed in the EUV spectrum of the control helium microwave discharge cell emission.

The EUV spectra (17.5 – 50 *nm*) of the microwave cell emission of the helium-hydrogen mixture (98/2%) (top curve) and the helium control (bottom curve) are shown in Figure 4. Ordinary hydrogen has no emission in these regions. Novel peaks were observed at 45.6 *nm*, 37.4 *nm*, and 20.5 *nm* which do not correspond to helium. At the 1 Torr condition, additional novel peaks were observed in the short wavelength region (5 – 65 *nm*) at 14.15 *nm*, 13.03 *nm*, 10.13 *nm*, and 8.29 *nm* which do not correspond to helium as shown in Figure 4. Known He I lines which were used for calibration of the novel peak positions were observed at 58.4 *nm*, 53.7 *nm*, and 52.4 *nm*. It is proposed that the 30.4 *nm* peak shown in Figures 4 and 5 was not entirely due to the He II transition. In the case of the helium-hydrogen mixture, the ratio of 30.4 *nm* (40.8 *eV*) peak to the 25.6 *nm* (48.3 *eV*) peak was 10 compared to 5.4 for helium alone as shown in Figure 4 which implies only a minor He II transition contribution to the 30.4 *nm* peak.

It is proposed that the majority of the 91.2 *nm* peak was also due to a novel transition. At 20 Torr, the ratio of the Lyman β peak to the 91.2 *nm* peak of the helium-hydrogen plasma was 2 compared to 8 for each control hydrogen and xenon-hydrogen plasma which indicates that the majority of the 91.2 *nm* peak was due to a transition other than the binding of an electron by a proton.

The novel peaks fit two empirical relationships. In order of energy, the set comprising the peaks at 91.2 *nm*, 45.6 *nm*, 30.4 *nm*, 13.03 *nm*, 10.13 *nm*, and 8.29 *nm* correspond to energies of $q \cdot 13.6\ eV$ where $q = 1,2,3,7,9,11$. In order of energy, the set comprising the peaks at 37.4 *nm*, 20.5 *nm*, and 14.15 *nm* correspond to energies of $q \cdot 13.6 - 21.21\ eV$ where $q = 4,6,8$. These lines can be explained as electronic transitions to fractional Rydberg states of atomic hydrogen given by Eqs. (1) and (3) wherein the catalytic system involves helium ions because the second ionization energy of helium is 54.417 *eV*, which is equivalent to $2 \cdot 27.2\ eV$. In this case, 54.417 *eV* is transferred nonradiatively from atomic hydrogen to He^+ which is resonantly ionized. The electron decays to the $n = 1/3$ state with the

further release of $54.417\,eV$ which may be emitted as a photon. The catalysis reaction is

$$54.417\,eV + He^{+} + H\left[a_H\right] \rightarrow He^{2+} + e^{-} + H\left[\frac{a_H}{3}\right] + 108.8\,eV \tag{7}$$

$$He^{2+} + e^{-} \rightarrow He^{+} + 54.417\,eV \tag{8}$$

And, the overall reaction is

$$H\left[a_H\right] \rightarrow H\left[\frac{a_H}{3}\right] + 54.4\,eV + 54.4\,eV \tag{9}$$

Since the products of the catalysis reaction have binding energies of $m \cdot 27.2\,eV$, they may further serve as catalysts. Thus, further catalytic transitions may occur: $n = \frac{1}{3} \rightarrow \frac{1}{4}$, $\frac{1}{4} \rightarrow \frac{1}{5}$, and so on.

Electronic transitions to Rydberg states given by Eqs. (1) and (3) catalyzed by the resonant nonradiative transfer of $m \cdot 27.2\,eV$ would give rise to a series of emission lines of energies $q \cdot 13.6\,eV$ where q is an integer. It is further proposed that the photons that arise from hydrogen transitions may undergo inelastic helium scattering. That is, the catalytic reaction

$$H\left[a_H\right] \xrightarrow{He^{+}} H\left[\frac{a_H}{3}\right] + 54.4\,eV + 54.4\,eV \tag{10}$$

yields $54.4\,eV$ by Eq. (8) and a photon of $54.4\,eV$ ($22.8\,nm$). Once emitted, the photon may be absorbed or scattered. When this photon strikes $He\,(1s^2)$, $21.2\,eV$ may be absorbed in the excitation to $He\,(1s^1 2p^1)$. This leaves a $33.19\,eV$ ($37.4\,nm$) photon peak and a $21.2\,eV$ ($58.4\,nm$) photon from $He\,(1s^1 2p^1)$. Thus, for helium the inelastic scattered peak of $54.4\,eV$ photons from Eq. (7) is given by

$$E = 54.4\,eV - 21.21\,eV = 33.19\,eV\ (37.4\,nm) \tag{11}$$

A novel peak shown in Figures 4 and 5 was observed at $37.4\,nm$. Furthermore, the intensity of the $58.4\,nm$ peak corresponding to the spectra shown in Figure 5 was about 60,000 photons/sec. Thus, the transition $He\,(1s^2) \rightarrow He\,(1s^1 2p^1)$ dominated the inelastic scattering of EUV peaks. The general reaction is

$$photon\,(h\nu) + He\,(1s^2) \rightarrow He\,(1s^1 2p^1) + photon\,(h\nu - 21.21\,eV) \tag{12}$$

The two empirical series may be combined—one directly from Eqs. (1, 3) and the other indirectly with Eq. (12). The energies for the novel lines in order of energy are $13.6\,eV$, $27.2\,eV$, $40.8\,eV$, $54.4\,eV$, $81.6\,eV$, $95.2\,eV$, $108.8\,eV$, $122.4\,eV$ and $149.6\,eV$. The corresponding peaks are $91.2\,nm$,

45.6 *nm*, 30.4 *nm*, 37.4 *nm*, 20.5 *nm*, 13.03 *nm*, 14.15 *nm*, 10.13 *nm*, and 8.29 *nm*, respectively. Thus, the identified novel lines correspond to energies of $q \cdot 13.6\,eV$ where $q = 1,2,3,4,6,7,8,9,11$ or these lines inelastically scattered by helium atoms wherein $21.2\,eV$ was absorbed in the excitation of $He\,(1s^2)$ to $He\,(1s^1 2p^1)$. The values of q observed are consistent with those excepted based on Eq. (9) and the subsequent autocatalyzed reactions as discussed previously [7]. The satellite peak at 44.2 *nm* show in Figure 4 and 5 may be due to multipole coupling as discussed elsewhere [8]. There is remarkable agreement between the data and the proposed transitions to fractional Rydberg states and these lines inelastically scattered by helium according to Eq. (12). All other peaks could be assigned to He I, He II, second order lines, or atomic or molecular hydrogen emission. No known lines of helium or hydrogen explain the $q \cdot 13.6\,eV$ related set of peaks.

B. Comparison of the intensity of He I and He II peaks with the addition of hydrogen to a helium microwave plasma

The results of the addition of 5% hydrogen to a helium microwave plasma maintained in the Evenson cavity with a forward power of 100 W and a reflected power of 30 W is shown in Figure 6. The broad peaks with a separation of 1.185 eV in the 27-65 nm region that were observed with the addition of hydrogen to the helium plasma were discussed previously [9]. The He I emission dominated for pure helium; whereas, He II emission dominated with the addition of hydrogen as shown by the comparison of the intensity of the emission of the He II peak at 30.4 *nm* to that of the He I peak at 58.4 *nm*. The catalysis reaction of He^+ (Eqs. (7-9)) would give rise to increase in He II emission according to the reaction given by Eq. (8); however, the effect of the addition of hydrogen on the intensity of the He II peak before the addition of hydrogen as well as after depended on the tuning of the cavity. The electric field of the Evenson cavity can be increased with appropriate tuning [24-25]. This condition corresponded to a high forward as well as a high reflected power. The intensity of the $q \cdot 13.6\,eV$ related set of peaks, the Balmer line broadening, the elevated T_e, and the excess power measured on helium-hydrogen microwave plasmas given in Secs. 3A, 3D, 3D, and 3E, respectively, showed the same dependency.

C. Helium-hydrogen glow discharge emission spectrum

The EUV spectra ($90-130\,nm$) and ($400-520\,nm$) of the cell emission from the hydrogen plasma (dotted line) and the hydrogen plasma to which 5% helium was added (solid line) are shown in Figures 7 and 8, respectively. Upon the addition of 5% helium, the hydrogen Lyman and Balmer line emission intensity approximately doubled which is indicative of a more energetic plasma.

D. Line broadening and T_e measurements

The Doppler-broadened line shape for atomic hydrogen has been studied on many sources such as hollow cathode [26-27] and rf [28-29] discharges. The method of Videnovic et al. [26] was used to calculate the energetic hydrogen atom densities and energies from the width of the 656.3 nm Balmer α line emitted from the hydrogen and helium-hydrogen mixture (90/10%) microwave plasmas shown in Figure 9. Gigosos et al. [30] have published a literature review of this method. The average helium-hydrogen Doppler half-width of $0.52 \pm 5\%\,nm$ was not appreciably changed with pressure. The corresponding energy of $180-210\,eV$ and the number densities of $5\,X10^{14} \pm 20\%\,atoms/cm^3$, depending on the pressure, were significant compared to only $\approx 3\,eV$ and $7\,X10^{13}\,atoms/cm^3$ for pure hydrogen, even though 10 times more hydrogen was present. Only $\approx 3\,eV$ broadening was observed with xenon-hydrogen (90/10%) ruling out collisional broadening.

Similarly, the average electron temperature for helium-hydrogen plasma was $28{,}000 \pm 5\%\,K$. Whereas, the corresponding temperature of helium alone was only $6800 \pm 5\%\,K$, and hydrogen alone was $5500 \pm 5\%\,K$. No high electric field was present in our experiments.

We have assumed that Doppler broadening due to thermal motion was the dominant source to the extent that other sources may be neglected. This assumption was confirmed when each source was considered. In general, the experimental profile is a convolution of two Doppler profiles, an instrumental profile, the natural (lifetime) profile, Stark profiles, Van der Waals profiles, a resonance profile, and fine

structure. The contribution from each source was determined to be below the limit of detection [11-12].

Furthermore, no hydrogen species, H^+, H_2^+, H_3^+, H^-, H, or H_2, responds to the microwave field; rather, only the electrons respond. But, the measured electron temperature was about 1 eV; whereas, the measured H temperature was $180\text{-}210\,eV$. This requires that $T_H >>> T_e$. This result can not be explained by electron or external Stark broadening or electric field acceleration of charged species. The electron density was five orders of magnitude too low [11-12]. And, in microwave driven plasmas, there is no high electric field in a cathode fall region ($>1\,kV/cm$) to accelerate positive ions as proposed previously [26-29] to explain significant broadening in hydrogen containing plasmas driven at a high voltage electrodes. It is impossible for H or any H-containing ion which may give rise to H to have a higher temperature than the electrons in a microwave plasma. The observation of excessive Balmer line broadening in a microwave driven plasma requires a source of energy other than that provided by the electric field.

E. Power balance of the hydrogen microwave plasma

The thermogram, $T(t)$ response of the cell, with stirring only and with a constant input power to the high precision heater of 50 W is shown in Figure 10. The baseline corrected least squares fit of the slope, $\dot{T}(t)$, was $2.622\,X10^{-4}\,°C/s$, and the heat capacity determined from Eqs. (5-6) with $P_{ex}=0$, and $P_{in}=P_{out}=50\,W$ was $1.907\,X10^{5}\,J/°C$. Then the temperature response of the calorimeter for any case (Eq. (6)) was determined to be

$$\dot{T}(t)=\left(1.907\,X10^{5}\,J/°C\right)^{-1}\times P_{out} \qquad (13)$$

The $T(t)$ water bath response to stirring and then with selected panel meter readings of the constant forward and reflected microwave input power to krypton was recorded as shown in Figure 11. Using the corresponding $\dot{T}(t)$ in Eq. (13), the microwave input power was determined to be $8.1\pm$ 1 W. A helium-hydrogen (90/10%) mixture was run at the same microwave input power readings as the control which corresponded to $P_{in}=8.1\pm1\,W$ in Eq. (5). The $T(t)$ response was significantly increased for helium-hydrogen (90/10%) as shown in Figure

11. At 350 minutes, the pressure was changed from 0.5 torr to 0.29 torr. A slight increase in $\dot{T}(t)$ was observed at the lower pressure, possibly due to an increase in atomic hydrogen and He^+. The excess power was determined to be 21.9 ± 1 W from the corresponding $\dot{T}(t)$ using Eq. (13) and Eq. (5).

The sources of error were the error in the calibration curve (± 0.05 W) and the measured microwave input power (± 1 W). The propagated error of the calibration and power measurements was ± 1 W.

Given a helium-hydrogen (90/10%) flow rate of 10.0 sccm and an excess power of 21.9 W, energy balances of over $-2.9\,X\,10^4\ kJ/mole\ H_2$ $(150\ eV/H\ atom)$ were measured. The reaction of hydrogen to form water which releases $-241.8\ kJ/mole\ H_2$ $(1.48\ eV/H\ atom)$ is about 100 times less than that observed. The results indicate that once an atom given by Eqs (1) and (3) is formed by a catalyst, further catalytic transitions: $n = \frac{1}{3} \rightarrow \frac{1}{4}, \frac{1}{4} \rightarrow \frac{1}{5}$, and so on occur to a substantial extent. This is consistent with the previously given theory [7, 18], the reported series of lower-energy hydrogen lines with energies of $q \cdot 13.6\ eV$ where $q = 1,2,3,4,6,7,8,9,$ *or* 11 [6-8], and previous studies which show very large energy balances [6, 11].

4. Conclusion

We report that novel emission lines were observed with energies of $q \cdot 13.6\ eV$ where $q = 1,2,3,4,6,7,8,9,11$ or these lines inelastically scattered by helium atoms wherein $21.2\ eV$ was absorbed in the excitation of $He\,(1s^2)$ to $He\,(1s^1 2p^1)$. These lines were identified as transitions to fractional Rydberg states of atomic hydrogen. An extremely high hydrogen-atom temperature of $180\text{-}210\ eV$ was observed with the presence of helium ion catalyst only with hydrogen present. Similarly, the average electron temperature for helium-hydrogen plasma was high, 28,000 K, compared to 6800 K for helium alone.

The intensity of the emission of the He II peak at $30.4\ nm$ relative to that of the He I peak at $58.4\ nm$ increased with the addition of 5% hydrogen. The effect was dependent on the microwave field which increased the amount of He^+ in both cases. Similarly, hydrogen plasmas

became more energetic when helium was added as indicated by the intensification of the Lyman and Balmer emission. The results showed the effect of the presence of He^+ with atomic hydrogen and demonstrated the role of He^+ as a catalyst.

Using water bath calorimetry, excess power was observed from the helium-hydrogen plasma compared to control krypton plasma. For a 8.1 W input, the thermal output power of the helium-hydrogen plasma was measured to be 30.0 W corresponding to 21.9 W of excess power in 3 cm^3. The excess power density and energy balance were high, $7.3\ W/cm^3$ and $-2.9\ X10^4\ kJ/mole\ H_2$, respectively. The results indicate that a new power source based on the catalysis of atomic hydrogen is not only possible, but is it competitive with gas turbine combustion.

Acknowledgments

Special thanks to Y. Lu and T. Onuma for recording some spectra.

References

1. R. Mills, J. Dong, Y. Lu, "Observation of Extreme Ultraviolet Hydrogen Emission from Incandescently Heated Hydrogen Gas with Certain Catalysts", Int. J. Hydrogen Energy, Vol. 25, (2000), pp. 919-943.
2. R. Mills and M. Nansteel, P. Ray, "Argon-Hydrogen-Strontium Discharge Light Source", IEEE Transactions on Plasma Science, in press.
3. R. Mills, P. Ray, Spectroscopic Identification of a Novel Catalytic Reaction of Potassium and Atomic Hydrogen and the Hydride Ion Product, Int. J. Hydrogen Energy, Vol. 27, No. 2, February, (2002), pp. 183-192.
4. R. Mills, "Spectroscopic Identification of a Novel Catalytic Reaction of Atomic Hydrogen and the Hydride Ion Product", Int. J. Hydrogen Energy, Vol. 26, No. 10, (2001), pp. 1041-1058.
5. R. L. Mills, P. Ray, "A Comprehensive Study of Spectra of the Bound-Free Hyperfine Levels of Novel Hydride Ion $H^-(1/2)$, Hydrogen, Nitrogen, and Air", Int. J. Hydrogen Energy, in press.
6. R. L. Mills, P. Ray, B. Dhandapani, M. Nansteel, X. Chen, J. He, "Spectroscopic Identification of Transitions of Fractional Rydberg

States of Atomic Hydrogen", J. of Quantitative Spectroscopy and Radiative Transfer, in press.
7. R. Mills, P. Ray, "Spectral Emission of Fractional Quantum Energy Levels of Atomic Hydrogen from a Helium-Hydrogen Plasma and the Implications for Dark Matter", Int. J. Hydrogen Energy, Vol. 27, No. 3, pp. 301-322.
8. R. L. Mills, P. Ray, B. Dhandapani, J. He, "Spectroscopic Identification of Fractional Rydberg States of Atomic Hydrogen", J. of Phys. Chem. (letter), submitted.
9. R. Mills, P. Ray, "Vibrational Spectral Emission of Fractional-Principal-Quantum-Energy-Level Hydrogen Molecular Ion", Int. J. Hydrogen Energy, Vol. 27, No. 5, (2002), pp. 533-564.
10. R. Mills, T. Onuma, and Y. Lu, "Formation of a Hydrogen Plasma from an Incandescently Heated Hydrogen-Catalyst Gas Mixture with an Anomalous Afterglow Duration", Int. J. Hydrogen Energy, Vol. 26, No. 7, July, (2001), pp. 749-762.
11. R. L. Mills, P. Ray, "Substantial Changes in the Characteristics of a Microwave Plasma Due to Combining Argon and Hydrogen", New Journal of Physics, www.njp.org, Vol. 4, (2002), pp. 22.1-22.17.
12. R. L. Mills, P. Ray, B. Dhandapani, J. He, "Comparison of Excessive Balmer α Line Broadening of Glow Discharge and Microwave Hydrogen Plasmas with Certain Catalysts", J. of Applied Physics, submitted.
13. R. Mills, B. Dhandapani, M. Nansteel, J. He, A. Voigt, "Identification of Compounds Containing Novel Hydride Ions by Nuclear Magnetic Resonance Spectroscopy", Int. J. Hydrogen Energy, Vol. 26, No. 9, Sept. (2001), pp. 965-979.
14. R. Mills, B. Dhandapani, N. Greenig, J. He, "Synthesis and Characterization of Potassium Iodo Hydride", Int. J. of Hydrogen Energy, Vol. 25, Issue 12, December, (2000), pp. 1185-1203.
15. R. Mills, "Novel Inorganic Hydride", Int. J. of Hydrogen Energy, Vol. 25, (2000), pp. 669-683.
16. R. Mills, B. Dhandapani, M. Nansteel, J. He, T. Shannon, A. Echezuria, "Synthesis and Characterization of Novel Hydride Compounds", Int. J. of Hydrogen Energy, Vol. 26, No. 4, (2001), pp. 339-367.
17. R. Mayo, R. Mills, "Direct Plasmadynamic Conversion of Plasma Thermal Power to Electricity for Microdistributed Power Applications",

40th Annual Power Sources Conference, Cherry Hill, NJ, June 10-13, (2002), in press.

18. R. Mills, *The Grand Unified Theory of Classical Quantum Mechanics*, September 2001 Edition, BlackLight Power, Inc., Cranbury, New Jersey, Distributed by Amazon.com; posted at www.blacklightpower.com.
19. R. Mills, "The Grand Unified Theory of Classical Quantum Mechanics", Int. J. Hydrogen Energy, Vol. 27, No. 5, (2002), pp. 565-590.
20. R. Mills, The Nature of Free Electrons in Superfluid Helium--a Test of Quantum Mechanics and a Basis to Review its Foundations and Make a Comparison to Classical Theory, Int. J. Hydrogen Energy, Vol. 26, No. 10, (2001), pp. 1059-1096.
21. N. V. Sidgwick, *The Chemical Elements and Their Compounds*, Volume I, Oxford, Clarendon Press, (1950), p.17.
22. M. D. Lamb, *Luminescence Spectroscopy*, Academic Press, London, (1978), p. 68.
23. H. R. Griem, *Principles of Plasma Spectroscopy*, Cambridge University Press, (1987).
24. F. C. Fehsenfeld, K. M. Evenson, H. P. Broida, "Microwave discharges operating at 2450 MHz", Review of scientific Instruments, Vol. 35, No. 3, (1965), pp. 294-298.
25. B. McCarroll, "An improved microwave discharge cavity for 2450 MHz", Review of Scientific Instruments, Vol. 41, (1970), p. 279.
26. I. R. Videnovic, N. Konjevic, M. M. Kuraica, "Spectroscopic investigations of a cathode fall region of the Grimm-type glow discharge", Spectrochimica Acta, Part B, Vol. 51, (1996), pp. 1707-1731.
27. S. Alexiou, E. Leboucher-Dalimier, "Hydrogen Balmer-α in dense plasmas", Phys, Rev. E, Vol. 60, No. 3, (1999), pp. 3436-3438.
28. S. Djurovic, J. R. Roberts, "Hydrogen Balmer alpha line shapes for hydrogen -argon mixtures in a low-pressure rf discharge", J. Appl. Phys., Vol. 74, No. 11, (1993), pp. 6558-6565.
29. S. B. Radovanov, K. Dzierzega, J. R. Roberts, J. K. Olthoff, Time-resolved Balmer-alpha emission from fast hydrogen atoms in low pressure, radio-frequency discharges in hydrogen", Appl. Phys. Lett., Vol. 66, No. 20, (1995), pp. 2637-2639.
30. M. A. Gigosos, V. Cardenoso, "New plasma diagnosis tables of hydrogen

Stark broadening including ion dynamics", J. Phys. B: At. Mol. Opt. Phys., Vol. 29, (1996), pp. 4795-4838.

Figure Captions

Figure 1. The experimental set up comprising a microwave discharge gas cell light source and an EUV spectrometer which was differentially pumped.

Figure 2. The experimental set up of a discharge gas cell light source and a VUV spectrometer which was differentially pumped.

Figure 3. Schematic of the water bath calorimeter. The Evenson cavity and a plasma-containing section of the quartz tube were fitted with an water-tight stainless steel housing, and the housing and cell assembly were suspended by 4 support rods from an acrylic plate which held the cell vertically from the top of a water bath calorimeter.

Figure 4. The EUV spectra ($17.5-50\ nm$) of the microwave cell emission of the helium-hydrogen mixture (98/2%) (top curve) recorded at 20 Torr with a normal incidence EUV spectrometer and a CEM, and control helium (bottom curve) recorded at 20 Torr with a 4° grazing incidence EUV spectrometer and a CEM. Only known He I and He II peaks were observed with the helium control. Reproducible novel emission lines were observed at $45.6\ nm$ and $30.4\ nm$ with energies of $q \cdot 13.6\ eV$ where $q = 2\ or\ 3$ (Eqs. (1, 3)) and at $37.4\ nm$ and $20.5\ nm$ with energies of $q \cdot 13.6\ eV$ where $q = 4\ or\ 6$ that were inelastically scattered by helium atoms wherein $21.2\ eV$ was absorbed in the excitation of $He\ (1s^2)$ to $He\ (1s^1 2p^1)$ as proposed in Eq. (12).

Figure 5. The short wavelength EUV spectra ($5-50\ nm$) of the microwave cell emission of the helium-hydrogen mixture (98/2%) (top curve) and control hydrogen (bottom curve) recorded at 1 Torr with a normal incidence EUV spectrometer and a CEM. No hydrogen emission was observed in this region, and no instrument artifacts were observed. Reproducible novel emission lines were observed at $45.6\ nm$, $30.4\ nm$, $13.03\ nm$, $10.13\ nm$, and $8.29\ nm$ with energies of $q \cdot 13.6\ eV$ where $q = 2,3,7,9,\ or\ 11$ and at $37.4\ nm$, $20.5\ nm$, and $14.15\ nm$ with energies of $q \cdot 13.6\ eV$ where $q = 4,6,\ or\ 8$ that were inelastically scattered by helium atoms wherein $21.2\ eV$ was absorbed in the excitation of $He\ (1s^2)$ to $He\ (1s^1 2p^1)$ as proposed in Eq. (12). The peak at $13.03\ nm$ was observed as a weak shoulder on the $14.15\ nm$ peak, and has been observed in repeated (non-presented) spectra.

Figure 6. The EUV spectra ($20-62\,nm$) of the microwave cell plasma emission of the helium (dotted curve) and the helium-hydrogen mixture (95/5%) (solid curve) recorded at 1 Torr with a 4° grazing incidence EUV spectrometer and a CEM. The plasmas were maintained in the Evenson cavity with a forward power of 100 W and a reflected power of 30 W. The He I emission dominated for pure helium; whereas, He II emission dominated with the addition of hydrogen as shown by the comparison of the intensity of the He II peak at $30.4\,nm$ to that of the He I peak at $58.4\,nm$.

Figure 7. The EUV spectra ($90-130\,nm$) of the glow discharge light source emission from the hydrogen plasma (dotted line) and the hydrogen plasma to which 5% helium was added (solid line) which shows the increase in hydrogen L_α emission.

Figure 8. The EUV spectra ($400-520\,nm$) of the glow discharge light source emission from the hydrogen plasma (dotted line) and the hydrogen plasma to which 5% helium was added (solid line) which shows the increase in hydrogen B_β and B_γ emission.

Figure 9. The 656.3 nm Balmer α line width recorded with a high resolution ($\pm 0.006\,nm$) visible spectrometer on a helium-hydrogen (90/10%) and a hydrogen microwave discharge plasma. Significant broadening was observed corresponding to an average hydrogen atom temperature of $180-210\,eV$.

Figure 10. The thermogram, $T(t)$ response of the cell, with stirring only and with a constant input power to the high precision heater of 50 W. The baseline corrected least squares fit of the slope, $\dot{T}(t)$, was $2.622\,X\,10^{-4}\,°C/s$, and the heat capacity was determined to be $1.907\,X\,10^{5}\,J/°C$.

Figure 11. The $T(t)$ water bath response to stirring and then with selected panel meter readings of the constant forward and reflected microwave input power to krypton was recorded. The microwave input power was determined to be 8.1 ± 1 W. A helium-hydrogen (90/10%) mixture was run at identical microwave input power readings as the control, and the excess power was determined to be 21.9 ± 1 W from the $T(t)$ response.

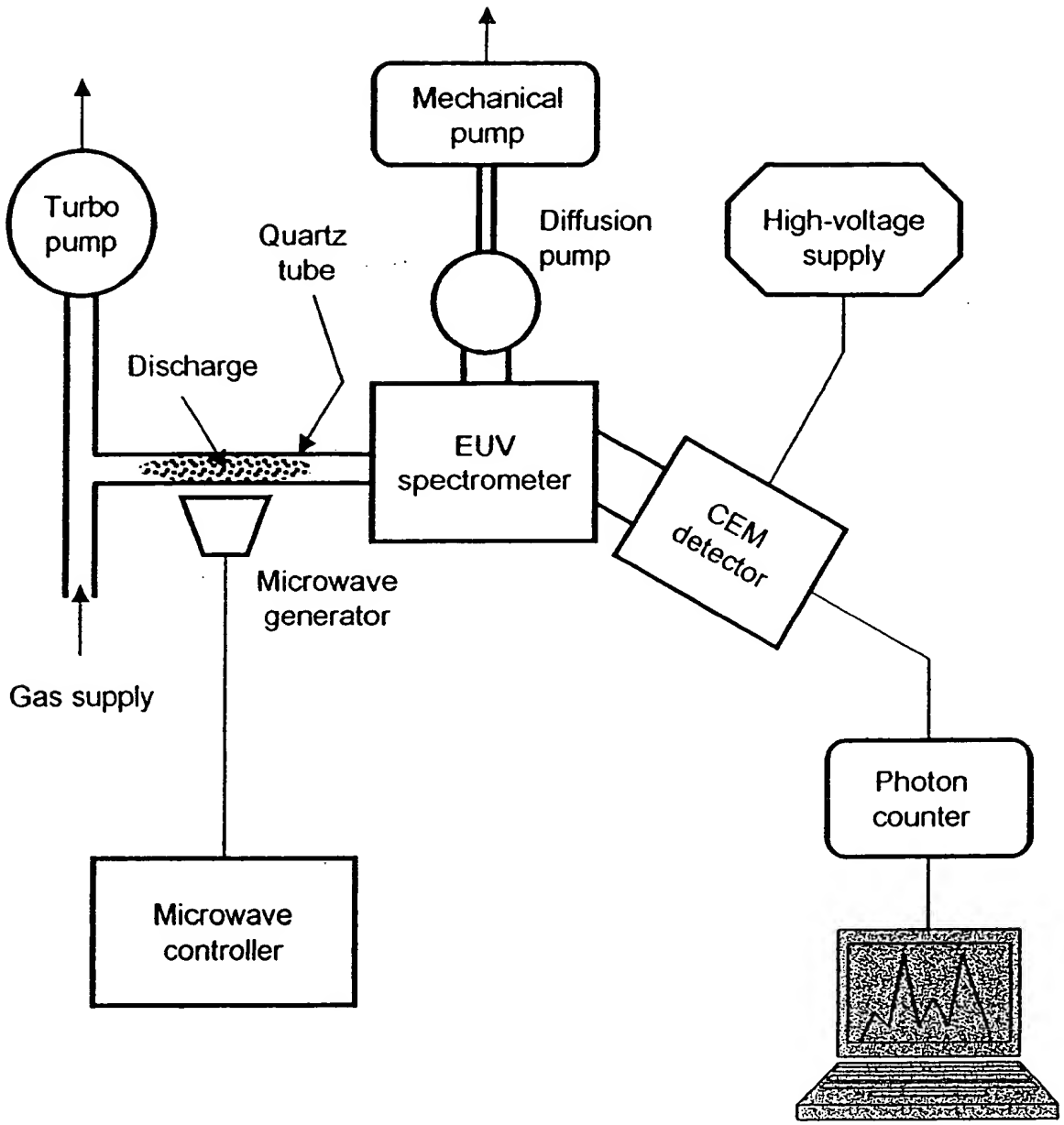
Mechanical pump
Turbo pump
Quartz tube
Diffusion pump
High-voltage supply
Discharge
EUV spectrometer
CEM detector
Microwave generator
Gas supply
Photon counter
Microwave controller

Fig. 1

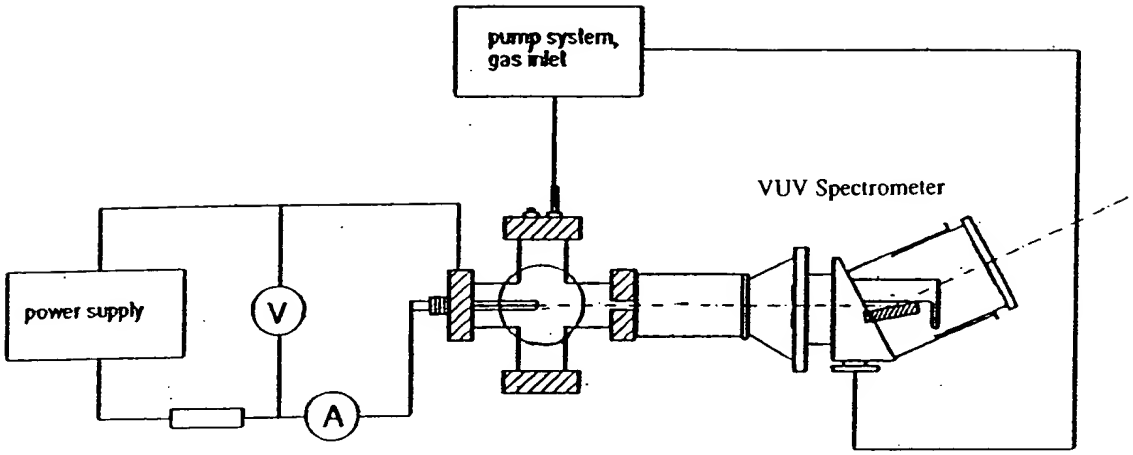

Fig. 2

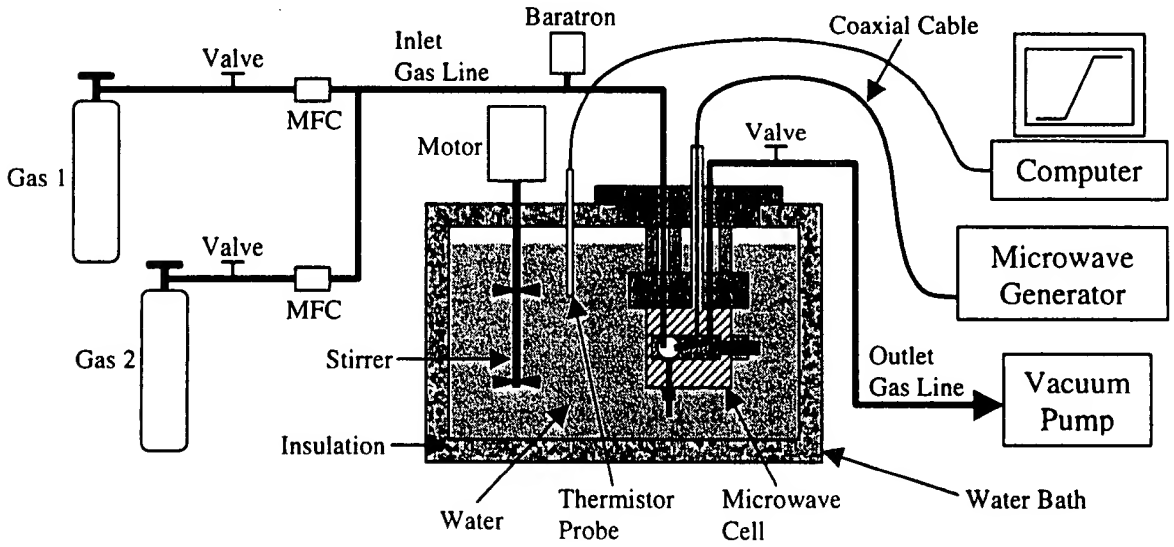
Baratron
Coaxial Cable
Valve
Inlet
Gas Line
MFC
Motor
Valve
Computer
Gas 1
Microwave
Generator
Valve
MFC
Gas 2
Stirrer
Outlet
Gas Line
Vacuum
Pump
Insulation
Water
Thermistor
Probe
Microwave
Cell
Water Bath

Fig. 3

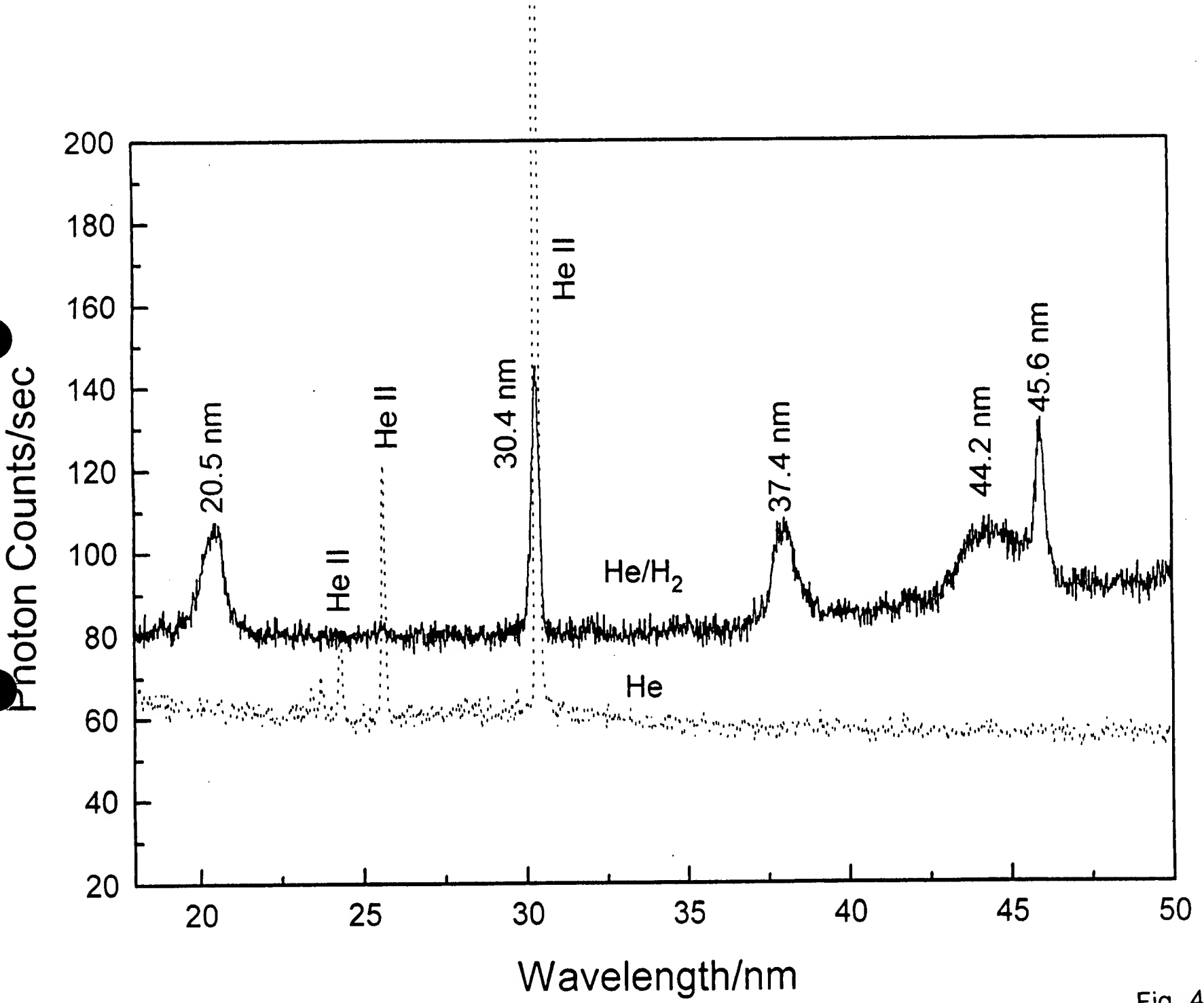
Photon Counts/sec
200
180
160
140
120
100
80
60
40
20
20.5 nm
He II
He II
30.4 nm
He II
He/H2
37.4 nm
44.2 nm
45.6 nm
He
20
25
30
35
40
45
50
Wavelength/nm

Fig. 4

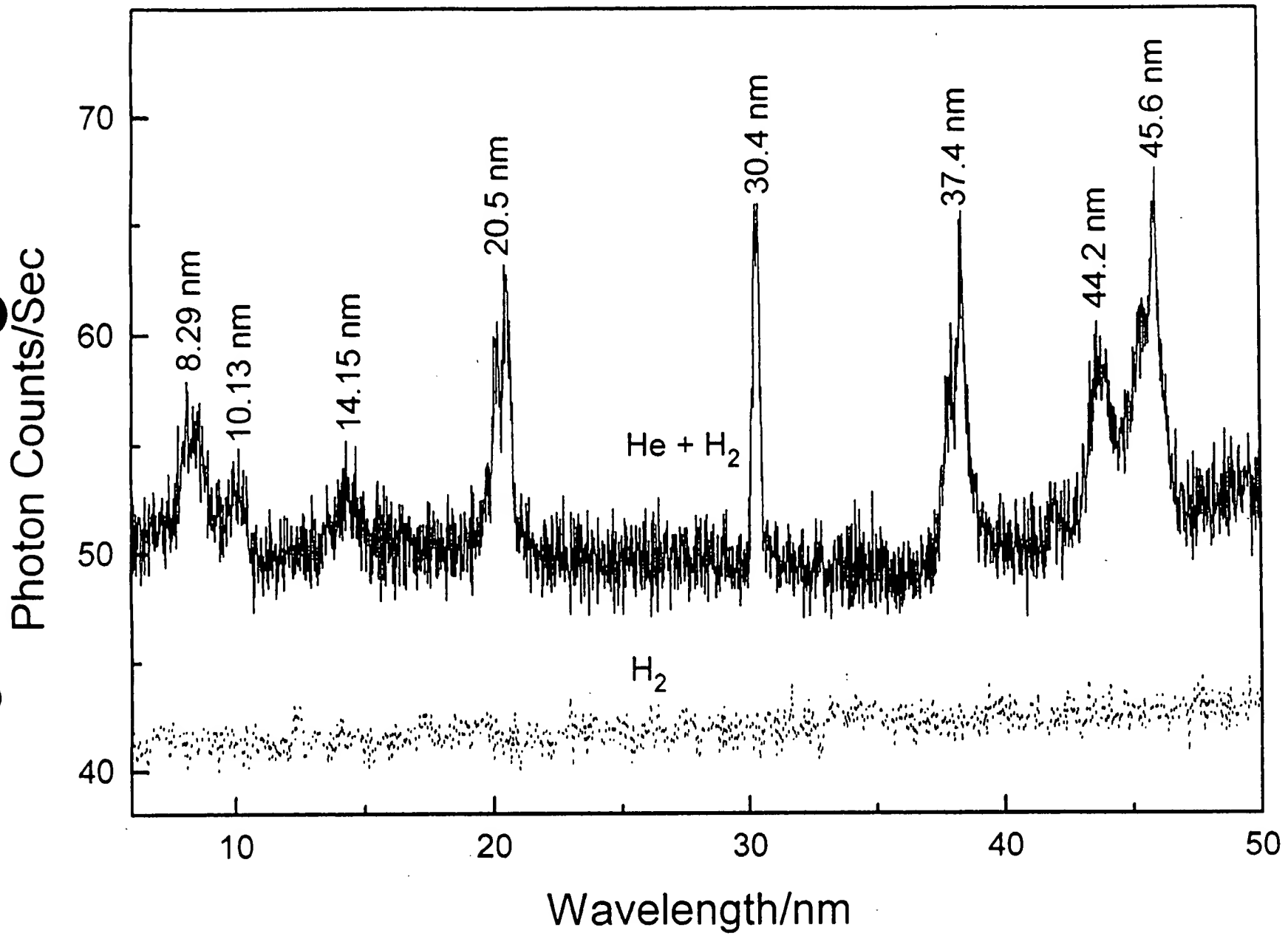
Photon Counts/Sec
70
60
50
40
8.29 nm
10.13 nm
14.15 nm
20.5 nm
30.4 nm
37.4 nm
44.2 nm
45.6 nm
He + H2
H2
10
20
30
40
50
Wavelength/nm

Fig. 5

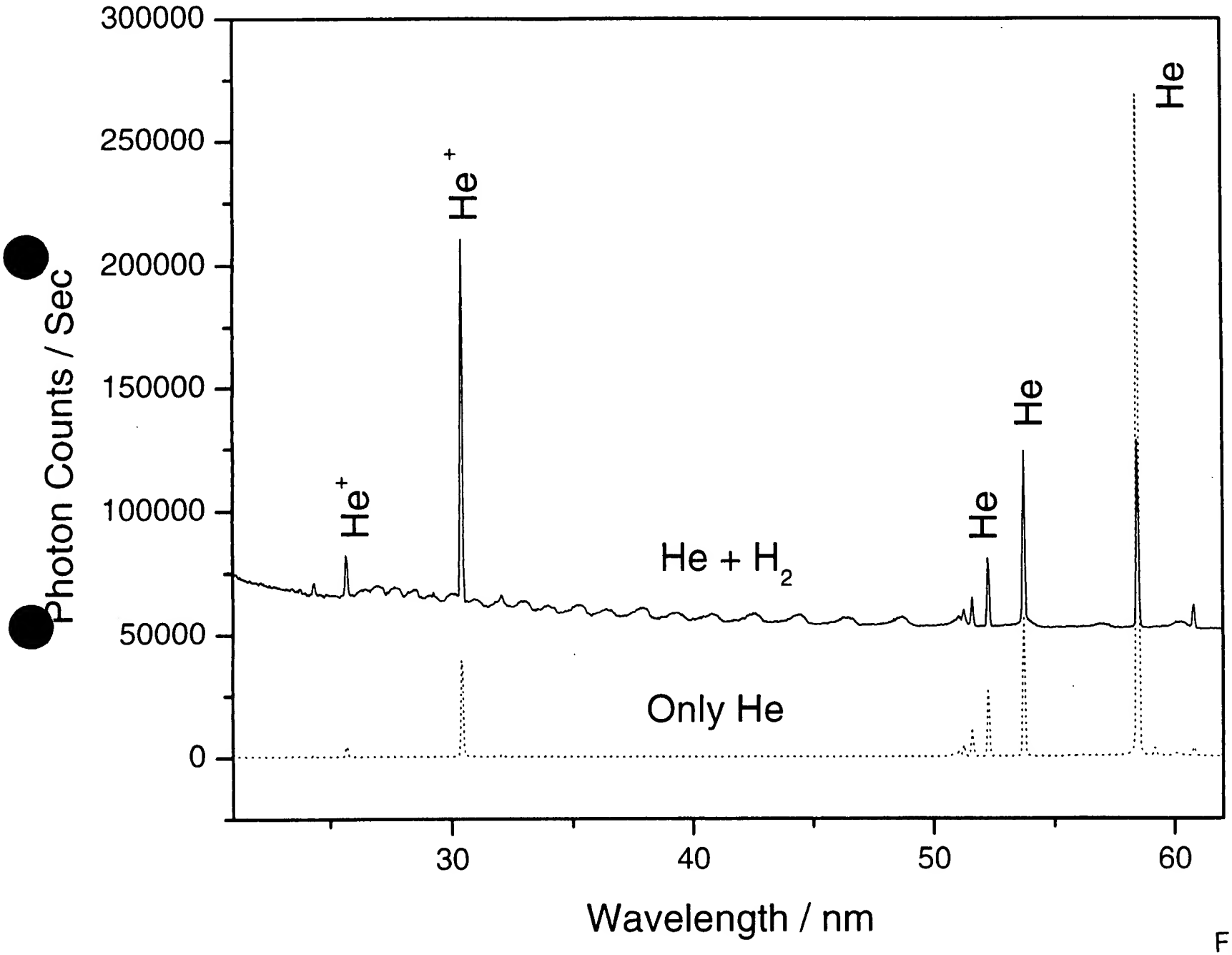
300000
250000
200000
150000
100000
50000
0
Photon Counts / Sec
30
40
50
60
Wavelength / nm
He+
He+
He
He
He
He + H2
Only He

Fig. 6

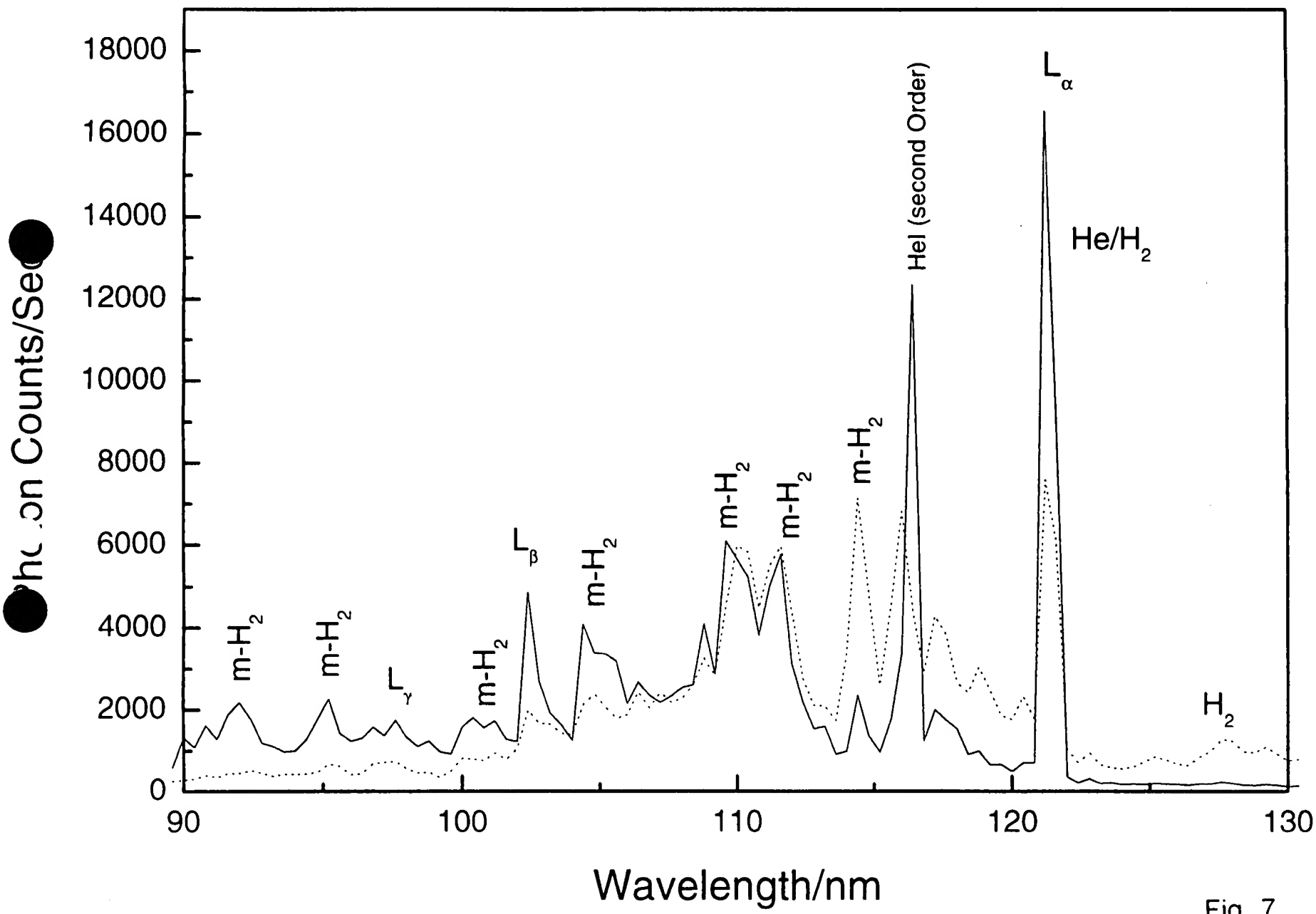
Photon Counts/Sec
18000
16000
14000
12000
10000
8000
6000
4000
2000
0
90
100
110
120
130
Wavelength/nm
m-H2
m-H2
Lγ
m-H2
Lβ
m-H2
m-H2
m-H2
m-H2
HeI (second Order)
Lα
He/H2
H2

Fig. 7

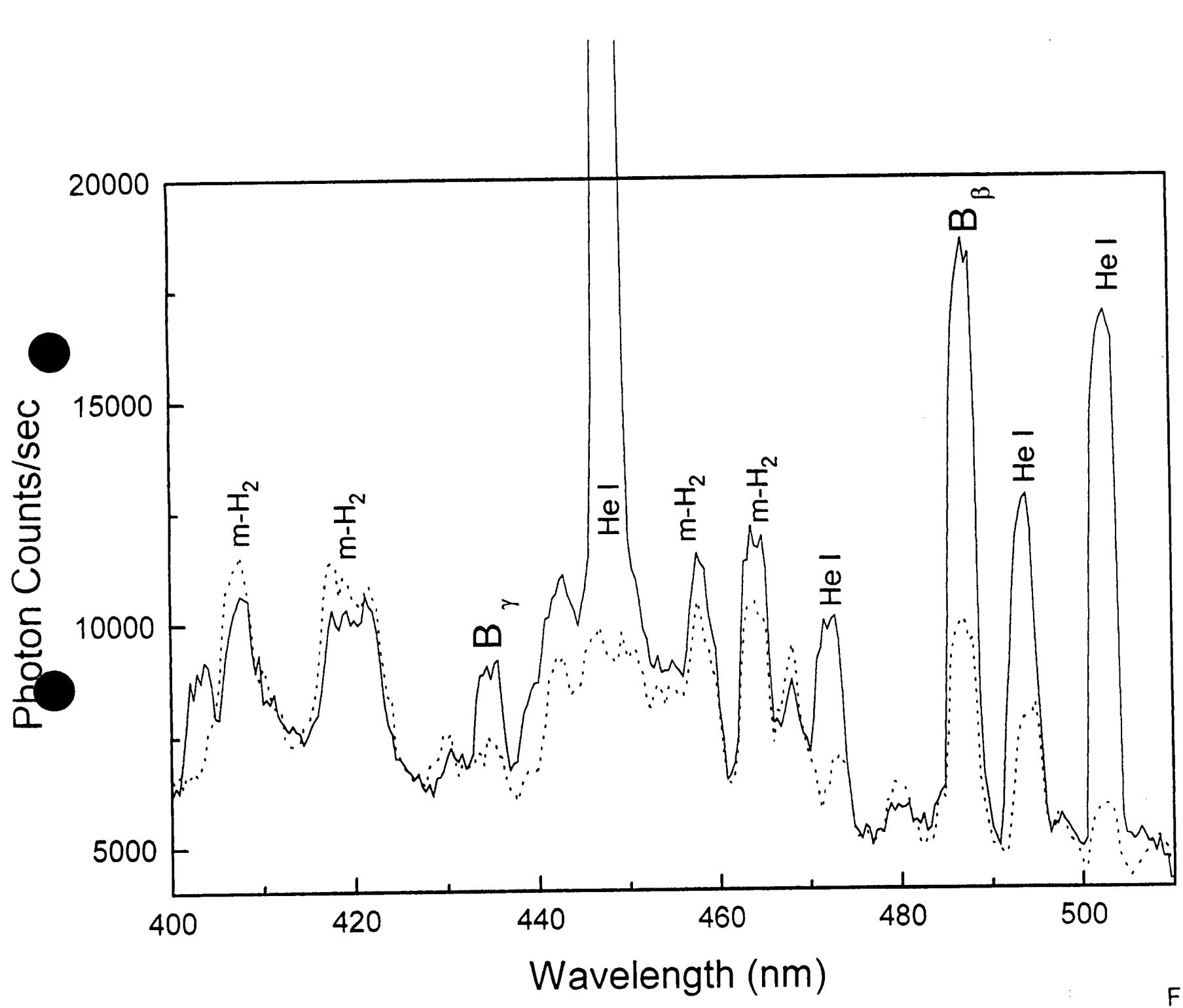
20000
15000
10000
5000
Photon Counts/sec
400
420
440
460
480
500
Wavelength (nm)
m-H2
m-H2
B γ
He I
m-H2
m-H2
He I
B β
He I
He I

Fig. 8

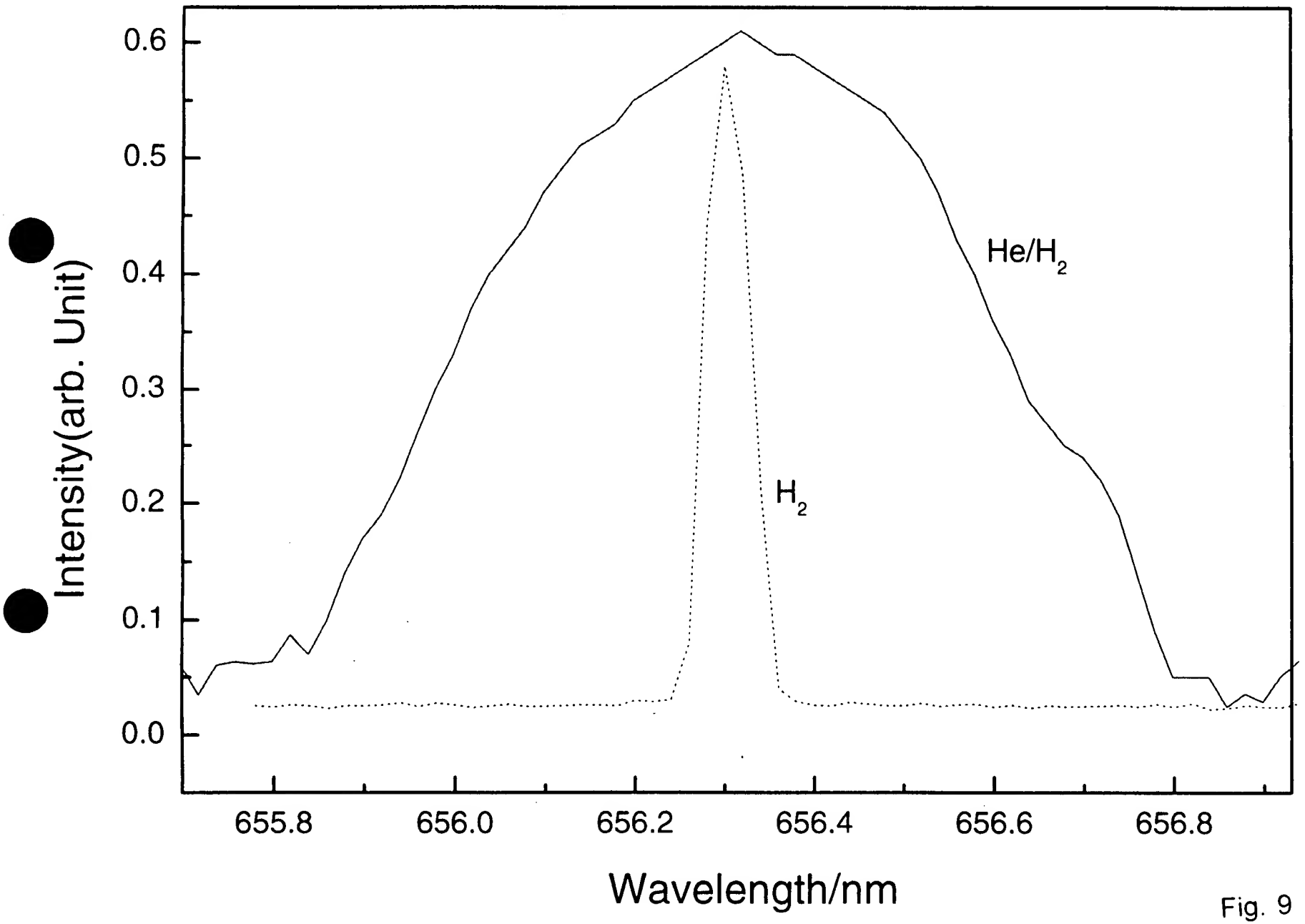
0.6
0.5
0.4
0.3
0.2
0.1
0.0
Intensity(arb. Unit)
He/H2
H2
655.8
656.0
656.2
656.4
656.6
656.8
Wavelength/nm

Fig. 9

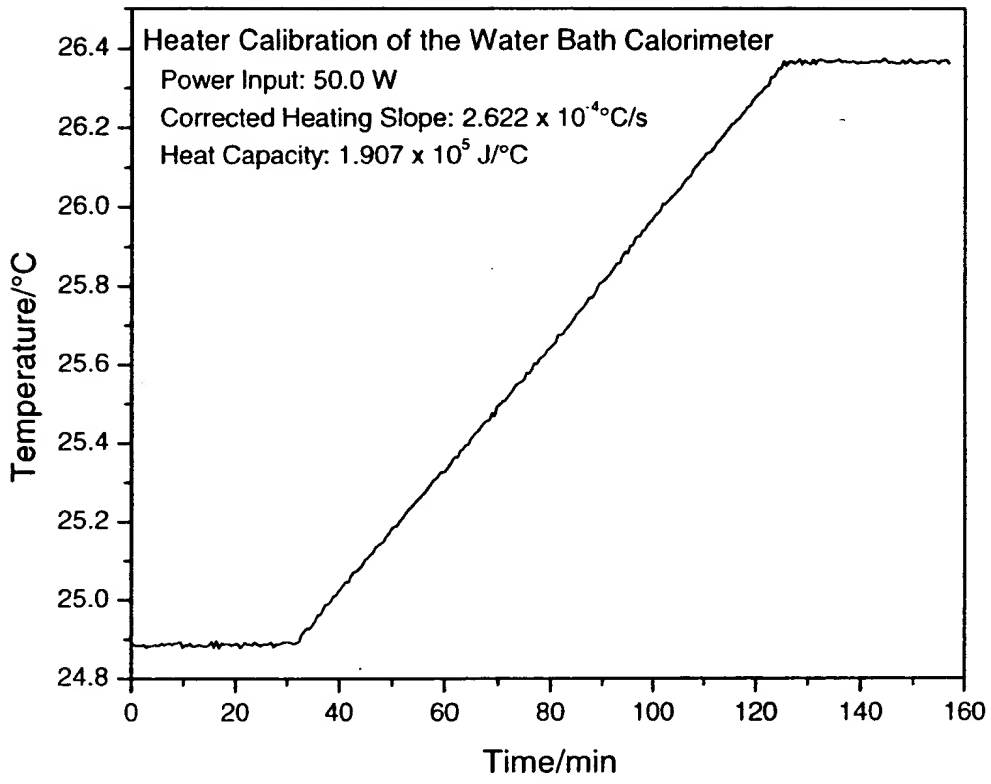
Heater Calibration of the Water Bath Calorimeter
Power Input: 50.0 W
Corrected Heating Slope: 2.622 x 10⁻⁴°C/s
Heat Capacity: 1.907 x 10⁵ J/°C
Temperature/°C
26.4
26.2
26.0
25.8
25.6
25.4
25.2
25.0
24.8
0
20
40
60
80
100
120
140
160
Time/min

Fig. 10

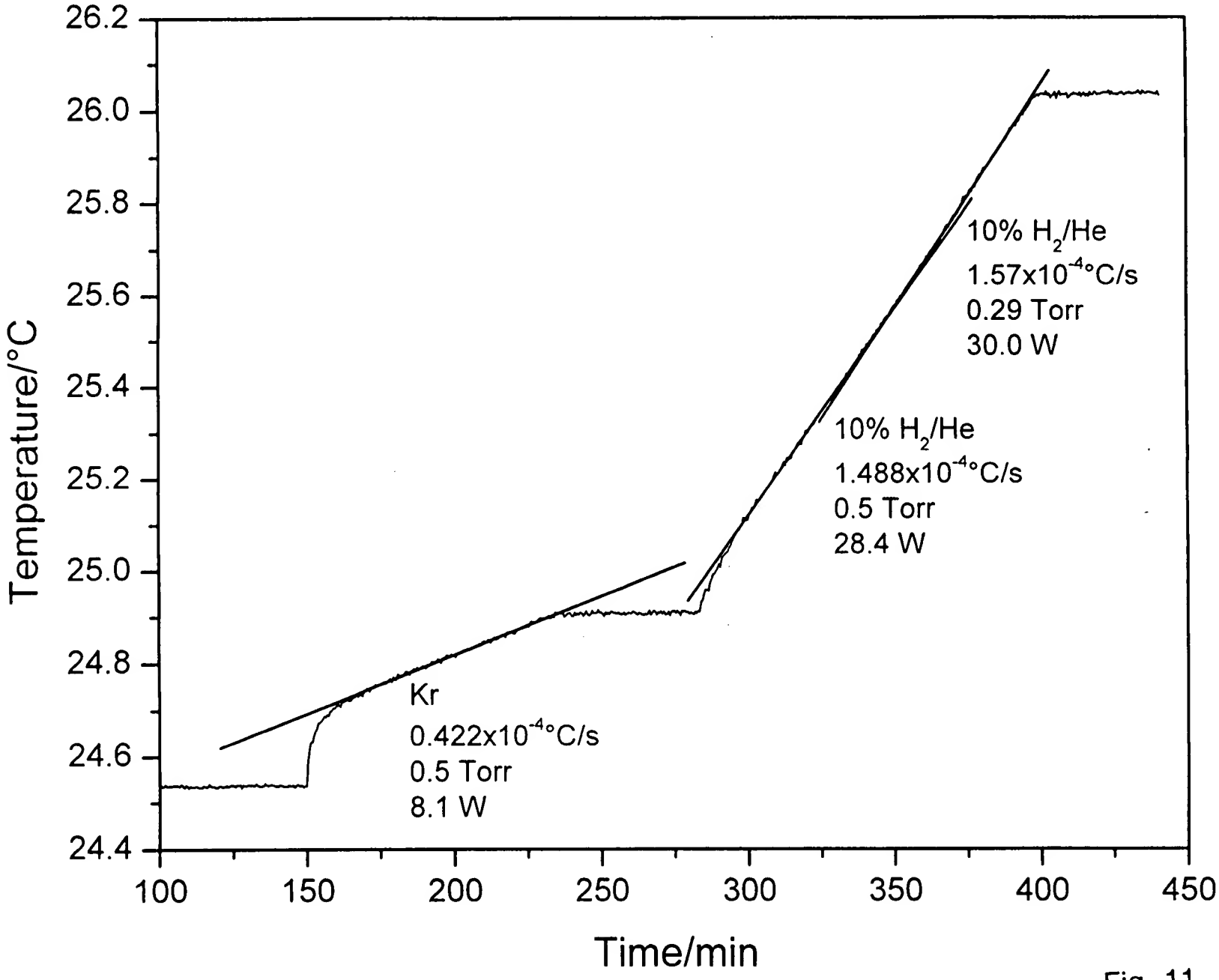
26.2
26.0
25.8
25.6
25.4
25.2
25.0
24.8
24.6
24.4
Temperature/°C
100
150
200
250
300
350
400
450
Time/min
10% H2/He
1.57x10-4°C/s
0.29 Torr
30.0 W
10% H2/He
1.488x10-4°C/s
0.5 Torr
28.4 W
Kr
0.422x10-4°C/s
0.5 Torr
8.1 W

Fig. 11